Oriented texture detection: Ideal observer modelling and classification image analysis

Charles C.-F. Or

Centre for Vision Research, York University, Toronto, ON, Canada

James H. Elder

Centre for Vision Research, York University, Toronto, ON, Canada

Perception of visual texture flows contributes to object segmentation, shape perception, and object recognition. To better understand the visual mechanisms underlying texture flow perception, we studied the factors limiting detection of simple forms of texture flows composed of local dot dipoles (Glass patterns) and related stimuli. To provide a benchmark for human performance, we derived an ideal observer for this task. We found that human detection thresholds were 8.0 times higher than ideal. We considered three factors that might account for this performance gap: (1) false matches between dipole dots (correspondence errors), (2) loss of sensitivity with increasing eccentricity, and (3) local orientation bandwidth. To estimate the effect of correspondence errors, we compared detection of Glass patterns with detection of matched line-segment stimuli, where no correspondence uncertainty exists. We found that eliminating correspondence errors reduced human thresholds by a factor of 1.8. We used a novel form of classification image analysis to directly estimate loss of sensitivity with eccentricity and local orientation bandwidth. Incorporating the eccentricity effects into the ideal observer model increased ideal thresholds by a factor of 2.9. Interestingly, estimated orientation bandwidth increased ideal thresholds by only 8%. Taking all three factors into account, human thresholds were only 58% higher than model thresholds. Our findings suggest that correspondence errors and eccentricity losses account for the great majority of the perceptual loss in the visual processing of Glass patterns.

Keywords: oriented texture, Glass pattern, ideal observer, classification image, reverse correlation

Citation: Or, C. C.-F., & Elder, J. H. (2011). Oriented texture detection: Ideal observer modelling and classification image analysis. *Journal of Vision, 11*(8):16, 1–20, http://www.journalofvision.org/content/11/8/16, doi:10.1167/11.8.16.

Introduction

Detection of oriented texture is an important problem, as it partially underlies our ability to segment figure from ground and perceive three-dimensional shape (Figure 1). This process involves perceptual organization of local orientation cues such that a coherent structure is perceived. A much-studied type of oriented texture is random dot-pair stimuli or Glass patterns (Glass, 1969; see Figures 2a and 2b). Perception of Glass patterns involves non-trivial processing: Local dots must be grouped appropriately to form perceptual pairs, and these pairs must be integrated to give a globally coherent orientation percept (Glass & Pérez, 1973; Glass & Switkes, 1976). Spurious orientation signals are formed when the dots are paired up randomly, which act as "correspondence errors" that limit detection performance. Given the apparent salience of Glass patterns, the visual system must have mechanisms that correlate the dots appropriately, minimizing random dot pairings.

The problem of detecting local orientations has been a central focus of neurophysiological research on the visual processing of Glass patterns. Glass (1969) proposed that each dipole (dot pair) is sufficient to trigger the response of a simple cell in V1 (Hubel & Wiesel, 1962, 1968) by activations of the two ends of its elongated receptive field. This idea was later supported by Smith, Bair, and Movshon (2002) and Smith, Kohn, and Movshon (2007) in monkey physiology, who found that neurons in V1 (and also V2) are sensitive to local orientations in linear Glass patterns.

How does the brain extract these weak orientation signals from Glass-pattern dipoles while suppressing spurious responses? Stevens (1978) proposed a token matching model that forms dipoles by detecting parallelism among local dot pairings. The model was designed such that dot pairings with smaller dot separations are preferred, and only dot pairings within a small neighbourhood of each dot are considered. The model predictions were generally consistent with human psychophysical data: In both cases, Glass patterns were detected only for small dipole lengths and low dot densities, to the extent that no more than 2 or 3 random dots could lie closer to a given dot than its corresponding dot (see also Caelli, 1981; Maloney, Mitchison, & Barlow, 1987). Contrary to Stevens' model, Dakin (1997) has found that a token matching model systematically underperforms humans on a Glass pattern detection task. Indeed, there is converging evidence that the structure of a Glass pattern is readily

doi: 10.1167/11.8.16 Received December 14, 2010; published July 27, 2011 ISSN 1534-7362 © ARVO

Downloaded from jov.arvojournals.org on 06/30/2019

Figure 1. The importance of texture flow perception. (a) Segmenting figure from ground: Detection of the squirrel is based in part on discriminating the texture flow of the animal's fur from the texture flow of the grass. (b) Perceiving three-dimensional shape from texture: The curvature of the chair is revealed by deformations in the texture flow of the chair's surface.

detectable for higher dot densities (relative to dipole length) than previously thought (Dakin, 1997; Kurki, Laurinen, Peromaa, & Saarinen, 2003; Wilson & Wilkinson, 1998; Wilson, Wilkinson, & Asaad, 1997).

The limitations of the token matching model suggest that local orientation signals may be extracted over larger spatial scales than previously thought. Dakin (1997) found that adaptive orientation filtering over multiple spatial scales agreed with human performance in detecting Glass patterns. Dakin and Bex (2001) further proposed that local grouping of dipoles is tuned to a narrow range of spatial frequencies, but global grouping is more broadly tuned. The need for a global pooling stage for linear Glass patterns is, however, disputed by Wilson and Wilkinson (1998) and Wilson et al. (1997), who found that spatial pooling of linear Glass patterns is limited to a relatively small foveal region.

To resolve this continuing debate, a better understanding of perceptual limits in the detection of Glass patterns is required. Early work focused largely on how correspondence errors alone limit perception of Glass patterns. For example, Maloney et al. (1987) examined the threshold signal-to-noise ratio of dots to perceive a Glass pattern when the average distance between dots was varied. Their model takes into account how the relative density of noise dots affects discriminability of the signal but does not allow investigation of other potential errors in the perception of oriented textures.

In order to more completely understand the perceptual factors determining the detection of texture flows, we conducted a new series of human psychophysical experiments using both linear Glass patterns (Figures 2a and 2b), as well as line patterns (Figures 2c and 2d) in which dipoles were replaced by line segments, which effectively eliminate the correspondence problem. Thus, the effect of correspondence errors can be measured by comparing the psychophysical thresholds for Glass patterns and line patterns. We further use a novel form of classification image analysis (Ahumada, 2002; Ahumada & Lovell, 1971) to examine three other potential sources of information loss: (1) decline in sensitivity with eccentricity (eccentricity loss) and two forms of orientation loss, including (2) bias in orientation detection and (3) orientation bandwidth (see Classification image analysis section). A main goal of our work is to establish a more comprehensive ideal observer model that provides a reference for human performance. Importantly, this model can be generalized to incorporate multiple forms of information loss that together limit detection performance.

Methods

Observers

Three experienced psychophysical observers participated in the experiments. Two of the observers (DN and YM) were naive to the purpose of the experiments, and the third observer (CFO) was one of the authors. All observers had normal, or corrected-to-normal, visual acuity.

Apparatus

Stimuli were generated using an Apple Power Macintosh G5 computer and MATLAB version 7.1 and were displayed on a 15-in. Apple colour monitor, at a frame rate of 85 Hz and a resolution of 1024 × 768 pixels. Observers viewed the monitor screen binocularly at a distance of

Downloaded from jov.arvojournals.org on 06/30/2019

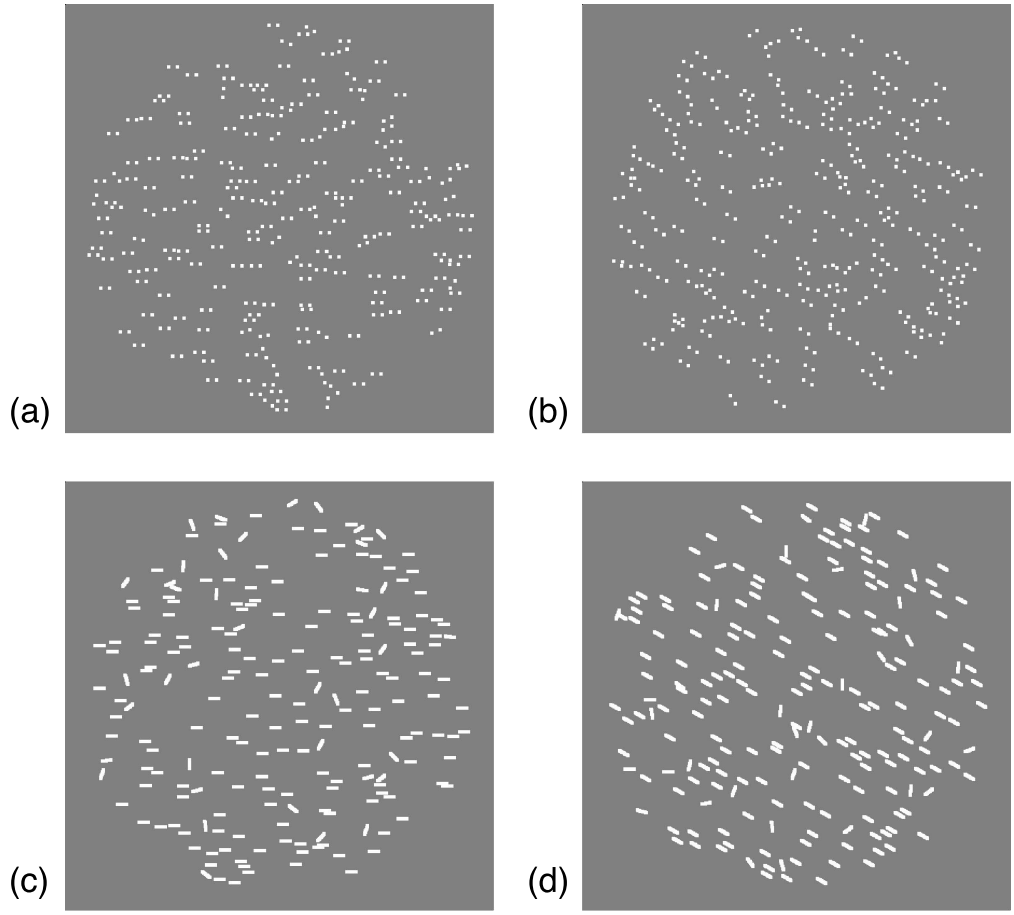

Figure 2. Noisy oriented texture stimuli. (a, b) Glass patterns. (c, d) Line patterns. Two signal orientations were used: 0 deg (horizontal; as in (a) and (c)) and 30 deg (oblique; as in (b) and (d)). Here, each of these sample oriented textures contains 80% signal.

70 cm in a dimly lit observation room. The monitor was gamma corrected by measuring the luminance of each RGB level with a Minolta LS-100 photometer, and then generating independent lookup tables for the red, green, and blue guns such that the screen luminance was linearized as a function of the grey level. Observers indicated their responses by pressing buttons on a standard keyboard.

Stimuli

Glass patterns

Each linear Glass pattern (Figures 2a and 2b) consisted of 200 dipoles. A dipole was produced by randomly positioning the first dot and placing its partner 19.2 min of arc away from the centre of the first dot. This dot-pair separation was within the range required for optimal detection of Glass pattern structure (Kurki et al., 2003; Wilson & Wilkinson, 1998). Each square dot had a size of 4.4 min of arc and was not allowed to overlap with any other dots. The dots were displayed within a circular aperture 14 deg in diameter, allowing eccentricity analysis in the parafoveal region. The dots were displayed at a luminance of 102 cd/m^2 against a background luminance of 60.3 cd/m^2.

As oblique Glass patterns have been found to result in better detection performance than horizontal or vertical (inverse oblique effect: Wilson, Loffler, Wilkinson, & Thistlethwaite, 2001), we ran separate experiments using horizontal (0 deg; see Figure 2a) and oblique (+30 deg; see Figure 2b) patterns. To construct a Glass pattern, a proportion of dipoles (signal dipoles) were oriented at the signal angle (0 deg or 30 deg). The orientations of the remaining dipoles (noise dipoles) were randomly distributed, with equal probability, over 6, 12, or 24 orientations evenly sampled from angles between −90 deg and 90 deg and including the signal angle. For example, the angles are −60, −30, 0, 30, 60, and 90 deg when 6 orientations are sampled. Figure 3 illustrates sample frequency distributions of dipole orientations in Glass patterns constructed by our method.

Line patterns

One possible factor underlying perceptual loss in Glass pattern detection is correspondence errors or errors in orientation detection arising from random correlations of local dots. This problem can be eliminated by replacing dipoles with oriented line segments. Dakin (1997) showed

Downloaded from jov.arvojournals.org on 06/30/2019

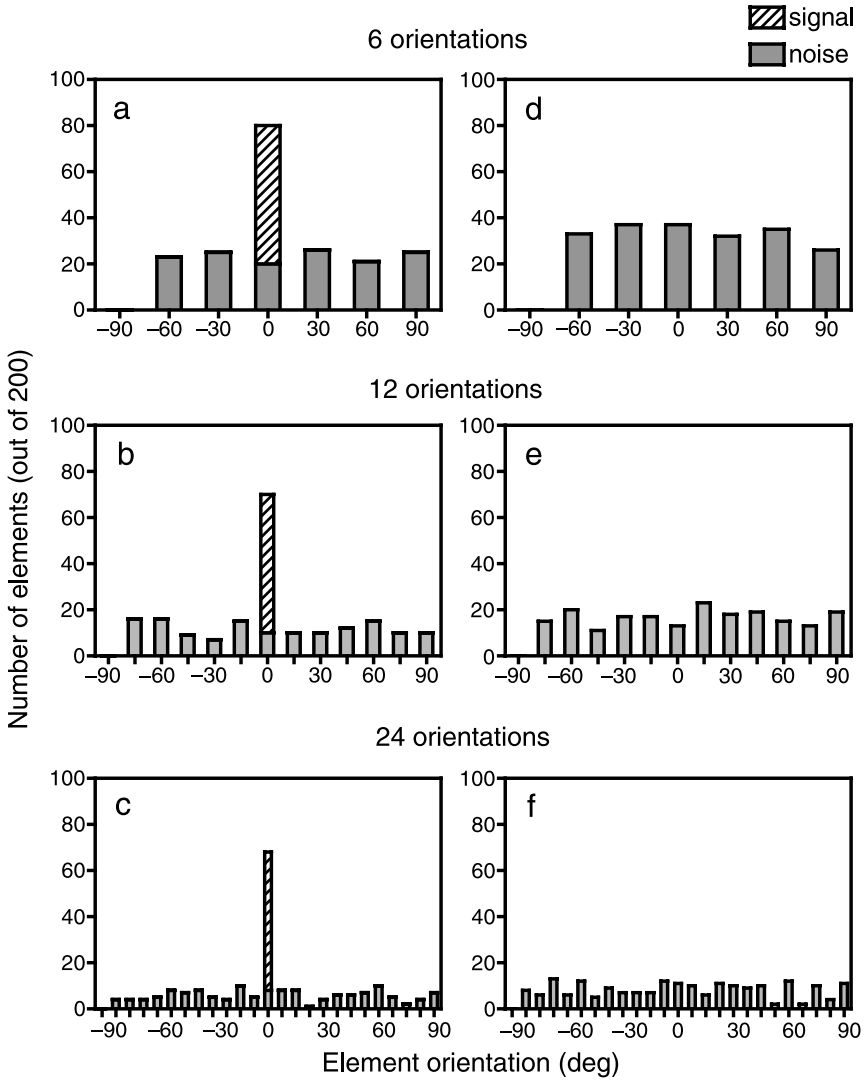

Figure 3. Sample frequency distributions of element orientations for oriented textures where the signal elements are oriented horizontally (at 0 deg). The numbers of orientations sampled are 6 (a, d), 12 (b, e), and 24 (c, f). (a–c) Signal-plus-noise patterns: Here, 30% of the 200 elements are deterministically set to the signal orientation. In actual experiments, signal level varied across trials. Note that the peaks are constituted of elements designated as signal (in stripes) and noise (in grey). (d–f) Noise-only patterns: All elements are oriented randomly.

that while detection of Glass patterns deteriorates beyond an optimal dipole length, detection of line patterns asymptotically improves with line length. Line patterns may also be useful in assessing information loss due to orientation tuning (Orientation loss section). For these reasons, we conducted our experiments also with line patterns (Figures 2c and 2d).

Line patterns were composed of 200 line segments, 4.4 × 22 min of arc in size, equivalent to the dipole dimensions of Glass patterns. Line segments were displayed at a luminance of 84.3 cd/m^2 against a background luminance of 60.3 cd/m^2. The lower luminance of line segments compared to dipoles (102 cd/m^2) equalized the total contrast energy of the two patterns. Pilot experiments revealed that in fact detection does not improve with contrast.

Procedure

A Yes/No detection task was used. On each trial, the observer was presented with a central fixation display for 1 s, followed by the target stimulus, centrally displayed for 165 ms (14 frames at 85 Hz), sufficiently brief to eliminate eye movements. The target stimulus on each trial was randomly either an oriented texture with a proportion of signal and noise elements (signal-plus-noise trial) or a pattern consisting of noise elements only (noise trial). The observer indicated by button press whether a presentation contained an oriented texture. The observer was notified of a correct or incorrect choice by an audible tone immediately after each decision.

Observers were tested, in a randomized order, in 12 conditions consisting of all combinations of three

Downloaded from jov.arvojournals.org on 06/30/2019

parameters: (1) stimulus type: Glass patterns or line patterns, (2) signal orientation: horizontal (0 deg) or oblique (30 deg) signal orientation, (3) number of distractor orientations: 6, 12, or 24. The observer was informed of these parameters at the start of each condition. Detection threshold for 75% correct performance was determined using an adaptive procedure (QUEST; Watson & Pelli, 1983; see Figure 11a). Each observer performed at least 2000 trials for each condition, in blocks of 200 trials each. (The exact number of blocks performed by each observer and for each condition varied slightly.) At the beginning of the first block, the initial signal level was set to 100 signal elements (50% signal) and the remaining 100 elements were noise elements. The initial signal level of each subsequent block was set to the maximum likelihood estimate of the detection threshold obtained from the previous block of the same condition. The mean detection threshold was calculated by averaging the maximum likelihood estimates of the detection thresholds obtained from all blocks for the same condition.

Ideal observer modelling

Since the retinal location of oriented elements is irrelevant to the task, the histogram of element orientations (Figure 3) completely embodies the stimulus information relevant to the task. We have also established that ideal observer thresholds for Glass patterns and line patterns are essentially identical, as the incidence of exact false dot matches is negligible at the dipole density (1.30 dipoles/deg^2 on average) we used.

As the signal orientation is known to the observer and the total number of elements is fixed at $N = 200$, the ideal observer only has to consider the number of elements at the signal orientation n_0. We make the further assumption that the ideal observer knows the signal level, i.e., the number n_s of elements deterministically set to the signal orientation on signal-present trials. (Note that the actual set of elements n_0 at the signal orientation consists of the signal elements plus the noise elements that happen to be at the signal orientation. See Figures 3a–3c.) This assumption is not unreasonable, as human thresholds are the outcome of a sequence of QUEST trials in which the signal level n_s gradually converges to a fixed value. Thus, in principle, it is possible for the ideal observer to develop a good estimate of the signal level n_s at its threshold. (In the Prior knowledge of signal level section, we explore how weaker knowledge of the signal level affects our analysis.)

In addition to knowledge of the signal level n_s, we assume that the ideal observer knows that the prior odds of signal present/absent is 50/50 and that the objective is to maximize proportion correct, consistent with a uniform reward for hits and correct rejects or equivalently a uniform loss for false positives and misses. With this knowledge, and an observed number of elements n_0 at the known signal orientation, the ideal observer reports the signal present if and only if this is the more likely event. Letting H_0 and H_1 denote the signal-absent and signal-present events, respectively, the decision rule can be written as

$$\begin{aligned} &\text{Decide } H_1 \quad \text{if } \frac{p(n_0|H_1, n_s)}{p(n_0|H_0)} \geq 1, \\ &\text{decide } H_0 \quad \text{otherwise.} \end{aligned} \tag{1}$$

Calculating the likelihood ratio is straightforward, since for both signal-present and signal-absent trials, n_0 follows a binomial distribution:

$$p(n_0|H_1, n_s) = \begin{cases} \binom{N - n_s}{n_0 - n_s} p_\theta^{n_0 - n_s} (1 - p_\theta)^{N - n_0}, & n_0 \geq n_s \\ 0, & n_0 < n_s \end{cases}, \tag{2}$$

$$p(n_0|H_0) = \binom{N}{n_0} p_\theta^{n_0} (1 - p_\theta)^{N - n_0}, \tag{3}$$

where $p_\theta = 1/n_\theta$ is the probability that a single noise element will have a particular orientation, given n_θ discrete stimulus orientations ($n_\theta = 6$, 12, or 24 in our experiments). The decision rule in Equation 1 then determines the ideal criterion n_0':

$$n_0' = \min_{n_0 \in [n_s, \ldots, N]} n_0 : \frac{p(n_0|H_1, n_s)}{p(n_0|H_0)} \geq 1. \tag{4}$$

In other words, n_0' is the minimum number of elements in the signal orientation for which the likelihood ratio equals or exceeds 1.

Given the optimal criterion n_0' as a function of signal level n_s, the proportion of correct responses p_c for every possible signal level $n_s \in [0, \ldots, N]$ (where $N = 200$) can be computed as the average of the hit rate p_{Hit} and correct-reject rate p_{CR}:

$$p_c(n_s) = \frac{1}{2}(p_{Hit}(n_s) + p_{CR}(n_s)), \tag{5}$$

where

$$p_{CR} = p(n_0 < n_0'|H_0) = \sum_{n_0=0}^{n_0'-1} \binom{N}{n_0} p_\theta^{n_0} (1 - p_\theta)^{N - n_0}, \tag{6}$$

Downloaded from jov.arvojournals.org on 06/30/2019

and

$$p_{\text{Hit}} = p(n_0 \geq n_0' | H_1, n_s) = \sum_{n_0=n_0'}^{N} \binom{N - n_s}{n_0 - n_s} p_\theta^{n_0 - n_s} (1 - p_\theta)^{N - n_0}. \quad (7)$$

Given the proportion of correct responses $p_c(n_s)$ for every integer signal level $n_s \in [0, \ldots, N]$, we compute the ideal threshold n_s' for 75% correct performance by linear interpolation.

Results

Figure 4 shows how detection thresholds vary as a function of our four factors: (1) observer (CFO, DN, or YM), (2) stimulus type (Glass patterns or line patterns), (3) signal orientation (horizontal or oblique), and (4) number

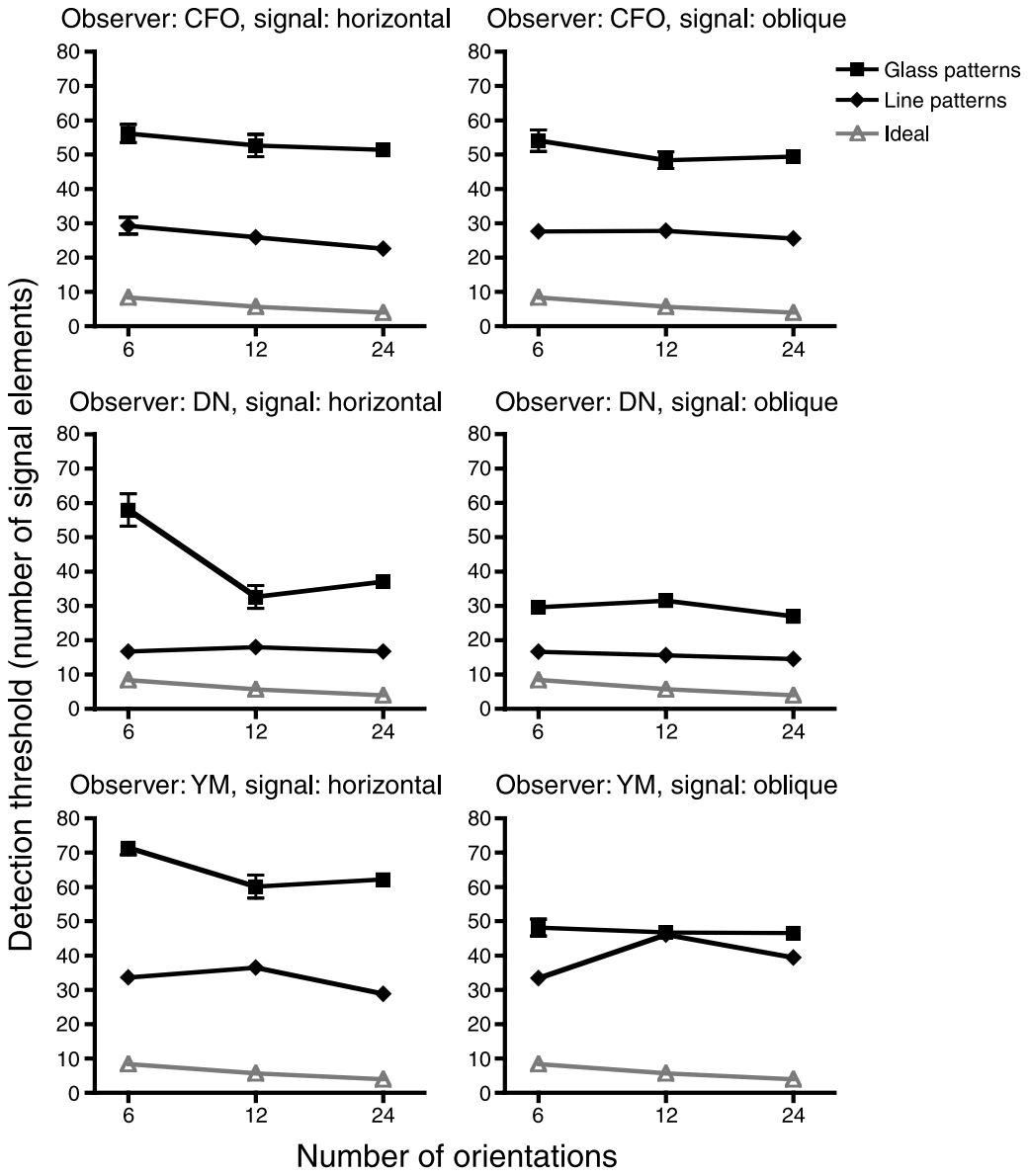

Figure 4. Detection thresholds as a function of observer, stimulus type (Glass pattern or line pattern), signal orientation, and number of orientations. Detection thresholds for the ideal observer are also shown. The threshold is expressed as the number of signal elements out of a total of 200 elements for 75% correct performance. Error bars denote ±1 *SEM*. Each mean and *SEM* is computed from at least 10 threshold estimates.

Downloaded from jov.arvojournals.org on 06/30/2019

Parameter	*F*	*df*	*P*-value
Main effects			
Observer (O)	250	2	<0.001
Signal orientation (SO)	38.7	1	<0.001
Stimulus type (ST)	879	1	<0.001
Number of orientations (NO)	12.9	2	<0.001
Two-way interactions			
O × SO	7.06	2	<0.001
O × ST	7.65	2	<0.001
O × NO	2.10	4	=0.080
SO × ST	81.9	1	<0.001
SO × NO	10.5	2	<0.001
ST × NO	14.2	2	<0.001
Three-way interactions			
O × SO × ST	17.2	2	<0.001
O × SO × NO	2.13	4	=0.077
O × ST × NO	2.60	4	<0.036
SO × ST × NO	2.39	2	=0.093
Four-way interactions			
O × SO × ST × NO	4.83	4	<0.001
Residual		394	

Table 1. Fixed-effects four-way ANOVA results on psychophysical detection threshold.

of orientations (6, 12, or 24). Table 1 shows the results of a fixed-effects four-way analysis of variance (ANOVA) on the detection thresholds based on these four factors. (We treat each 200-trial threshold estimate as an independent observation, yielding at least 10 observations per condition. Since the number of blocks performed by each observer and for each condition varies only slightly, the design is nearly balanced.)

We find that all main effects and most interactions are significant ($p < 0.05$). Since several of these significant interactions involve the observer factor, we also conducted three-way (conditional) ANOVAs for each observer (Table 2) to assess the generalization of observed effects across individuals. While a complete account of all higher order interactions is beyond the scope of this paper, we shall attempt to shed light at least on the main effects and selected two-way interactions in the following.

Our first observation is that observers varied significantly in how well they performed the oriented texture detection task. This may, in part, be due to individual differences in the parameters of detection mechanisms that we shall attempt to estimate in this paper; this possibility is reinforced by the significant interactions between observer and the stimulus parameters. For this reason, much of our subsequent analysis will be within subjects.

Our second observation is that, for all three observers, Glass patterns have significantly higher detection thresholds than line patterns, by a factor of 1.8 on average. This finding confirms that line patterns produce a stronger texture flow than Glass patterns, possibly due to the absence of correspondence errors in line patterns.

Our third observation is that, for two of our three observers, thresholds are significantly lower for oblique patterns than for horizontal patterns, consistent with previous findings (Wilson et al., 2001). We note that this inverse oblique effect is highly significant ($p < 0.001$) for the two observers who show it and nowhere near

Observer CFO

Parameter	*F*	*df*	*P*-value
Main effects			
Signal orientation (SO)	0.324	1	=0.570
Stimulus type (ST)	305	1	<0.001
Number of orientations (NO)	3.35	2	<0.038
Two-way interactions			
SO × ST	1.69	1	=0.196
SO × NO	0.252	2	=0.778
ST × NO	0.423	2	=0.656
Three-way interactions			
SO × ST × NO	0.354	2	=0.703
Residual		138	

Observer DN

Main effects			
Signal orientation (SO)	44.6	1	<0.001
Stimulus type (ST)	313	1	<0.001
Number of orientations (NO)	13.6	2	<0.001
Two-way interactions			
SO × ST	27.7	1	<0.001
SO × NO	10.9	2	<0.001
ST × NO	11.7	2	<0.001
Three-way interactions			
SO × ST × NO	15.5	2	<0.001
Residual		108	

Observer YM

Main effects			
Signal orientation (SO)	22.8	1	<0.001
Stimulus type (ST)	305	1	<0.001
Number of orientations (NO)	3.32	2	<0.040
Two-way interactions			
SO × ST	115	1	<0.001
SO × NO	7.45	2	<0.001
ST × NO	11.6	2	<0.001
Three-way interactions			
SO × ST × NO	0.284	2	=0.753
Residual		148	

Table 2. Three-way conditional ANOVA results on psychophysical detection threshold for three observers. Residual *df* varies slightly because each observer performed a slightly different number of blocks for some conditions.

Downloaded from jov.arvojournals.org on 06/30/2019

significant ($p = 0.57$) for the third observer. This finding suggests that the inverse oblique effect may only hold for a subset of the population, although clearly a larger sample size is required to substantiate this claim.

Our fourth observation is that there is a general decline in thresholds as the number of orientations in the stimulus is increased, statistically significant in all three observers ($p < 0.04$). Note that the decline in thresholds is predicted by the ideal observer model and reflects the decline in the number of noise elements at the signal orientation as the number of orientations in the stimulus increases.

Our final observation is that thresholds for the ideal observer are considerably lower than for human observers, even when correspondence errors have been accounted for (using line patterns). Clearly, there are other important sources of information loss in the detection of oriented textures: we now set out to identify and quantify these losses.

Classification image analysis

Prior work has suggested that the detection of oriented textures is limited by (1) decline in sensitivity with eccentricity (eccentricity loss; Burr & Ross, 2006; Dakin, 2001; Wilson & Wilkinson, 1998; Wilson et al., 1997) and (2) bias and bandwidth in detecting the orientation of the global structure (orientation loss; Dakin, 1997, 2001; Maloney et al., 1987). Unfortunately, a full-scale comparison of the magnitudes of these errors is impossible due to different experimental settings in past studies. More importantly, estimations of the eccentricity loss and orientation loss in past studies generally involved strong assumptions about the detection mechanism. For example, eccentricity loss was estimated by comparing detection thresholds of Glass patterns of different sizes (Wilson & Wilkinson, 1998; Wilson et al., 1997) under the assumption that sensitivity at a specific eccentricity is not affected by changes in stimulus size.

Here, we use a classification image technique (Ahumada, 2002; Ahumada & Lovell, 1971) that allows more direct estimation of both eccentricity loss and orientation loss. These estimates are based only on signal-absent trials: we excluded signal-present trials to avoid possible biases toward the signal due to system non-linearities (Abbey & Eckstein, 2002; Ahumada & Beard, 1999). (Nevertheless, we have verified that including signal-present trials produces similar results.)

(Since our analyses will generally be in one-dimensional subspaces of the image, specifically, in orientation and eccentricity bands, rather than the pixel domain, we will be estimating one-dimensional sensitivity functions rather than "classification images" per se. However, in the visual psychophysics community, the term "classification image" is used quite broadly to describe any internal template estimated using stimulus noise under a linear signal detection model, and this is the sense in which we use the term.)

Eccentricity loss

Background

It is well known that visual performance generally decreases with retinal eccentricity due to optical (Campbell & Green, 1965; Fincham, 1951) and neural (Cowey & Rolls, 1974; Daniel & Whitteridge, 1961; De Monasterio & Gouras, 1975; Wiesel, 1960) factors. In particular, orientation sensitivity has been shown to deteriorate in the periphery (Spinelli, Bazzeo, & Vicario, 1984).

It is to be expected that the decay in sensitivity with eccentricity will limit the detection of oriented textures. However, the rate of decay is disputed. While Wilson and Wilkinson (1998) and Wilson et al. (1997) found that detection of linear Glass patterns does not improve with increased stimulus size beyond fovea, Burr and Ross (2006) found otherwise. For Gabor textures, Dakin (2001) found only a slight improvement in detection with a larger stimulus area. The effect of eccentricity loss in oriented texture detection thus merits further investigation.

Here, we used the classification image technique to directly measure observers' sensitivity to orientation information at different spatial locations relative to fixation. The decay in element sensitivity with eccentricity was estimated from the resulting sensitivity function.

Methods

A sensitivity function for signal-absent trials was determined by comparing the eccentricities of noise elements at the signal orientation in false-alarm and correct-reject trials. In particular, a sensitivity estimate can be computed by accumulating noise elements into discrete eccentricity bins for false-alarm and correct-reject trials separately, and then differencing the normalized bins to produce an empirical estimate of the sensitivity function C_r at discrete eccentricity bins i:

$$C_r(i) = \frac{1}{n_{FA}} N_{FA}(i) - \frac{1}{n_{CR}} N_{CR}(i), \quad (8)$$

where n_{FA} is the number of false-alarm trials, n_{CR} is the number of correct-reject trials, $N_{FA}(i)$ is the number of elements falling in eccentricity bin i over all false-alarm trials, and $N_{CR}(i)$ is the number of elements falling in eccentricity bin i over all correct-reject trials.

Note that Equation 8 can be rewritten as

$$C_r(i) = \sum_{j=1}^{N_i} w_{ij}, \quad (9)$$

Downloaded from jov.arvojournals.org on 06/30/2019

where w_{ij} is a weight assigned to the jth element falling in bin i:

$$w_{ij} = \frac{1}{n_{\mathrm{FA}}} \quad \text{if the element is drawn from a false-alarm trial,}$$

$$w_{ij} = -\frac{1}{n_{\mathrm{CR}}} \quad \text{if the element is drawn from a correct-reject trial,} \tag{10}$$

and N_i is the number of elements falling in bin i over all (signal-absent) trials.

This empirical estimate of the sensitivity function will only be accurate if each bin contains (roughly) the same number of elements. Since the expected number of elements falling within a fixed tolerance of a given eccentricity r increases as r^2, the bin width is made to decrease as $\sqrt{r}$ such that the expected number of elements is the same across the bins. Figure 5a shows the empirical eccentricity sensitivity function computed in this fashion for one observer and signal orientation.

It would be nice to capture this falloff in sensitivity with a simple parametric model. Prior studies have suggested an exponential falloff in sensitivity with eccentricity, for a range of perceptual tasks (Robson & Graham, 1981; Spinelli et al., 1984). Thus, we predict that our empirical sensitivity function will be well approximated by the following function:

$$\hat{C}_{\mathrm{r}}(r) = A_{\mathrm{r}}\exp(-r/r_0), \tag{11}$$

where r is the eccentricity of an element, defined as the angular deviation of the element's midpoint from fixation, and r_0 is the space constant for the falloff.

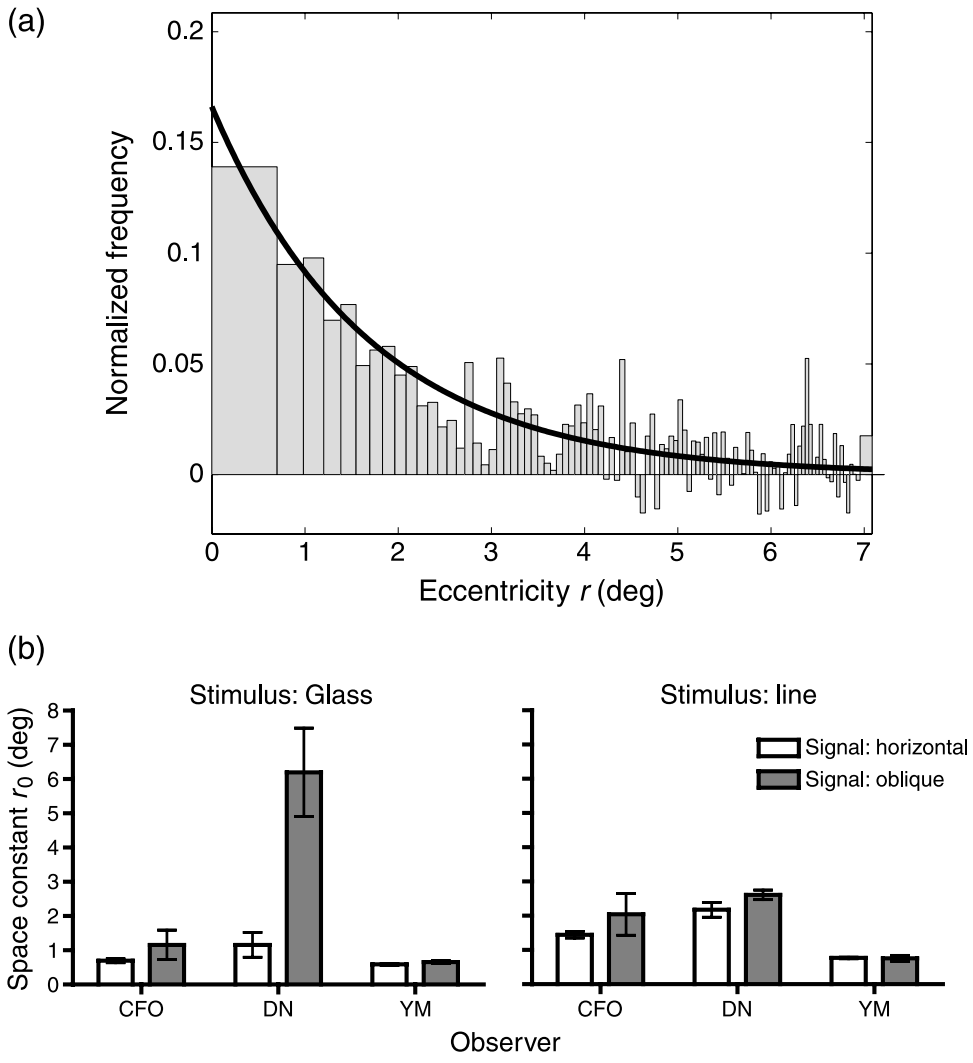

Figure 5. (a) Empirical sensitivity function over eccentricity for observer DN on horizontal textures. Here, we used 100 histogram bins, each containing 1186 elements on average. The curve shows the maximum likelihood exponential model $\hat{C}_{\mathrm{r}}(r) = A_{\mathrm{r}}\exp(-r/r_0)$. (b) Mean eccentricity space constants. Error bars denote ±1 *SEM*. Each mean and *SEM* is derived from three estimates: one for each of the three values of the number of orientations factor.

Downloaded from jov.arvojournals.org on 06/30/2019

While our binning method provides a good visualization of the falloff in sensitivity $C_r(r)$ with eccentricity r, a least-squares fit of our model $\hat{C}_r(r)$ directly to this empirical sensitivity function $C_r(r)$ is sensitive to the choice of the bin width. We can eliminate this dependence by using one bin per oriented texture element, centring each on the eccentricity of that element, and making the bin widths so small that they each encompass only one point. It is important to note that there may be gaps and overlaps between the bins, but this is not a problem, since our goal is only to estimate the sensitivity at a discrete number of r values, not to estimate a probability density. Under these conditions, the number of bins is equal to the total number of elements and the estimated sensitivity at the ith bin is given by

$$C_r(i) = w_{ij}, \tag{12}$$

with w_{ij} defined as in Equations 9 and 10. Now a least-squares fit of the model $\hat{C}_r(r)$ to the data can be computed by minimizing

$$\begin{aligned} L &= \sum_{i=1}^{N} (\hat{C}_r(i) - C_r(i))^2 \\ &= \sum_{i=1}^{N} (\hat{C}_r(i) - w_{ij})^2 \\ &= \sum_{i \in I_{FA}} \left(\hat{C}_r(i) - \frac{1}{n_{FA}} \right)^2 + \sum_{i \in I_{CR}} \left(\hat{C}_r(i) + \frac{1}{n_{CR}} \right)^2, \end{aligned} \tag{13}$$

where I_{FA} and I_{CR} are the index sets for all noise elements in the false-alarm and correct-reject trials, respectively. We minimize Equation 13 over A_r and r_0 using a standard gradient descent method (MATLAB *fminsearch*). We report only the results for r_0, since A_r is an arbitrary scaling constant.

The fit of the exponential model to the data using this method is good, yielding parameters similar to those estimated by fitting histograms (Figure 5a), and we have verified that it is better than an alternative half-normal model.

Results

Table 3 shows the results of a fixed-effects four-way ANOVA on estimated space constant r_0 as a function of our four factors: (1) observer (CFO, DN, or YM), (2) stimulus type (Glass patterns or line patterns), (3) signal orientation (horizontal or oblique), and (4) number of orientations (6, 12, or 24). We find significant main effects of observer and signal orientation as well as three significant two-way interactions (observer × signal orientation, observer × stimulus type, stimulus type × signal orientation) and one significant three-way interaction (observer × stimulus type × signal orientation). (Given only one estimate per condition, the fourth-order interaction is undefined.) As there is no significant effect of the number of orientations, either as a main effect or in interactions, we averaged the space constants over the three values of this factor (Figure 5b).

Parameter	*F*	*df*	*P*-value
Main effects			
Observer (O)	36.6	2	<0.003
Signal orientation (SO)	22.6	1	<0.009
Stimulus type (ST)	0.228	1	=0.658
Number of orientations (NO)	1.62	2	=0.306
Two-way interactions			
O × SO	13.0	2	<0.018
O × ST	7.19	2	<0.048
O × NO	1.13	4	=0.455
SO × ST	10.8	1	<0.031
SO × NO	0.879	2	=0.483
ST × NO	0.472	2	=0.654
Three-way interactions			
O × SO × ST	11.2	2	<0.024
O × SO × NO	0.790	4	=0.588
O × ST × NO	3.19	4	=0.143
SO × ST × NO	0.046	2	=0.956
Residual		4	

Table 3. Fixed-effects four-way ANOVA results on estimated eccentricity space constant.

In all but one case, space constants were between 0.6 and 2.6 deg. The average space constant was 1.7 deg. Ignoring the one outlier estimate (observer DN, oblique Glass patterns), the average space constant was 1.3 deg. For horizontal Glass patterns, we found an average space constant for our exponential model of 0.81 deg. Wilson and Wilkinson (1998) have previously estimated sensitivity to comparable stimuli as a function of eccentricity by measuring thresholds for circular regions of various sizes. Using a half-normal model, they estimated a space constant of 0.65 deg. To compare our exponential model with their half-normal model, we can compute for both the eccentricities at which sensitivity falls to half its peak value. Our estimate of 0.56 deg is almost identical to the 0.54-deg estimate obtained by Wilson and Wilkinson using quite different methods. The agreement in these estimates strengthens the conclusion that sensitivity to Glass patterns is largely restricted to the central 1-deg region of the visual field.

From Figure 5b, we observe that in 5 out of 6 cases, the estimated space constant is greater for the oblique signal orientation, as reflected in the significant main effect of signal orientation. This means that overall our observers are closer to ideal for the oblique condition in the sense that they are using more of the information in the display. This is one possible explanation for the effect of signal orientation on performance observed in Figure 4. Note

Downloaded from jov.arvojournals.org on 06/30/2019

that these differences parallel the space constant estimates shown in Figure 5b fairly closely. For example, observer DN is much better for oblique signals, at least for the 6-orientation condition, and this is where we see the largest difference in estimated space constants. The one case in which the estimated space constant is (slightly) smaller for the oblique condition (observer YM, line patterns) is the one case where performance is worse for the oblique condition. The individual differences we observe here may partly explain variations in previous estimates of eccentricity decay (Burr & Ross, 2006; Dakin, 2001; Wilson & Wilkinson, 1998; Wilson et al., 1997).

These results are also consistent with previous findings from Wilson et al. (2001), who measured thresholds for oblique Glass patterns while varying stimulus area, finding broader spatial pooling for oblique patterns. What remains unclear is the functional role for this broader pooling and how it relates to the ecological statistics of natural oriented textures.

Orientation loss

Background

Neurons in early visual cortex are tuned for orientation (Hubel & Wiesel, 1962, 1968) and underlie our ability to perceive oriented patterns. Psychophysical estimates of orientation bandwidths for gratings generally range from 7 to 15 deg, half-width at half-height (Blakemore & Nachmias, 1971; Campbell & Kulikowski, 1966; Phillips & Wilson, 1984; Snowden, 1992). Orientation bandwidths of oriented textures probably fall within this range. Maloney et al. (1987) found that Glass patterns are still visible even with ±11-deg jitter in dipole orientations, and Dakin (1997, 2001) found similar results for line patterns and Gabor textures. Nevertheless, some of these estimates may be confounded with other potential errors in oriented texture detection, notably correspondence errors in Glass patterns: errors in orientation detection in Glass patterns may arise from both random dot correlations and imprecise orientation tuning. Fortunately, the classification image technique allows these sources of error to be studied.

Methods

Our analysis of eccentricity showed that elements near fixation are far more influential in determining oriented texture detection, and we can take this into account to improve our estimates of orientation bandwidth. Specifically, let $I_{FA}(\theta)$ and $I_{CR}(\theta)$ denote index sets for all noise elements at orientation θ in false-alarm and correct-reject trials, respectively. Then, the empirical sensitivity function over orientation is

$$C_\theta(\theta) = \frac{1}{n_{FA}} \sum_{i \in I_{FA}(\theta)} \exp(-r_i/r_0) - \frac{1}{n_{CR}} \sum_{i \in I_{CR}(\theta)} \exp(-r_i/r_0), \quad (14)$$

where r_i is the eccentricity of noise element i, r_0 is the space constant estimated separately for each observer and stimulus parameter (Eccentricity loss section), and n_{FA} and n_{CR} are the numbers of false-alarm and correct-reject trials, respectively. In this way, elements that are closer to fixation and have greater influence on detection are weighted more heavily in estimating the orientation bandwidth.

The empirical sensitivity functions over orientation are shown in Figure 6. Note that sensitivity peaks near the signal orientation and has negative tails. This is in part due to the nature of the stimuli: The fact that every stimulus contains exactly 200 elements means that the empirical sensitivity function must sum to zero.

To parametrically model orientation tuning, we fit the empirical sensitivity function with a Gaussian function, corrected to have zero sum:

$$\hat{C}_\theta(\theta) = A_\theta \left[\frac{1}{\sqrt{2\pi}\sigma_\theta} \exp\left(\frac{-(\theta - \mu_\theta)^2}{2\sigma_\theta^2} \right) - 1 \right]. \quad (15)$$

The standard deviation σ_θ provides an estimate of the orientation bandwidth for oriented texture detection. The difference between the mean μ_θ and the signal orientation θ_0 (i.e., $\mu_\theta - \theta_0$) indicates observer bias. We compute error estimates for the orientation bandwidth σ_θ as 68% confidence intervals based on 500 bootstrapped estimates.

Results

Figure 6 shows that orientation bandwidths in the classification images are generally too narrow to be estimated accurately from 6- and 12-orientation stimuli. We thus base all of our analysis on the 24-orientation results by performing a fixed-effects three-way ANOVA (factors: observer, stimulus type, signal orientation) separately on the observer biases $\mu_\theta - \theta_0$ and bandwidths σ_θ of the Gaussian functions fit to the empirical sensitivity functions over orientation. The statistical results reported below are based on ANOVA models without interaction terms, all of which were found to be not significant ($p > 0.12$) in the full models.

For observer bias, no significant differences were found for observer, $F(2,7) = 2.37$, $p = 0.16$, stimulus type, $F(1,7) = 0.632$, $p = 0.45$, or signal orientation, $F(1,7) = 1.30$, $p = 0.29$. Importantly, an additional t-test reveals an average bias of -0.22 deg not significantly different from zero bias, $t(11) = 0.322$, $p = 0.75$ (two-tailed).

For orientation bandwidth, no consistent evidence was found for different orientation bandwidths for Glass patterns and line patterns, $F(1,7) = 2.75$, $p = 0.14$. This finding suggests that superior performance for detection of line patterns derives mainly from elimination of correspondence errors, not a reduction in orientation loss. It also suggests that local orientation processing is similar

Downloaded from jov.arvojournals.org on 06/30/2019

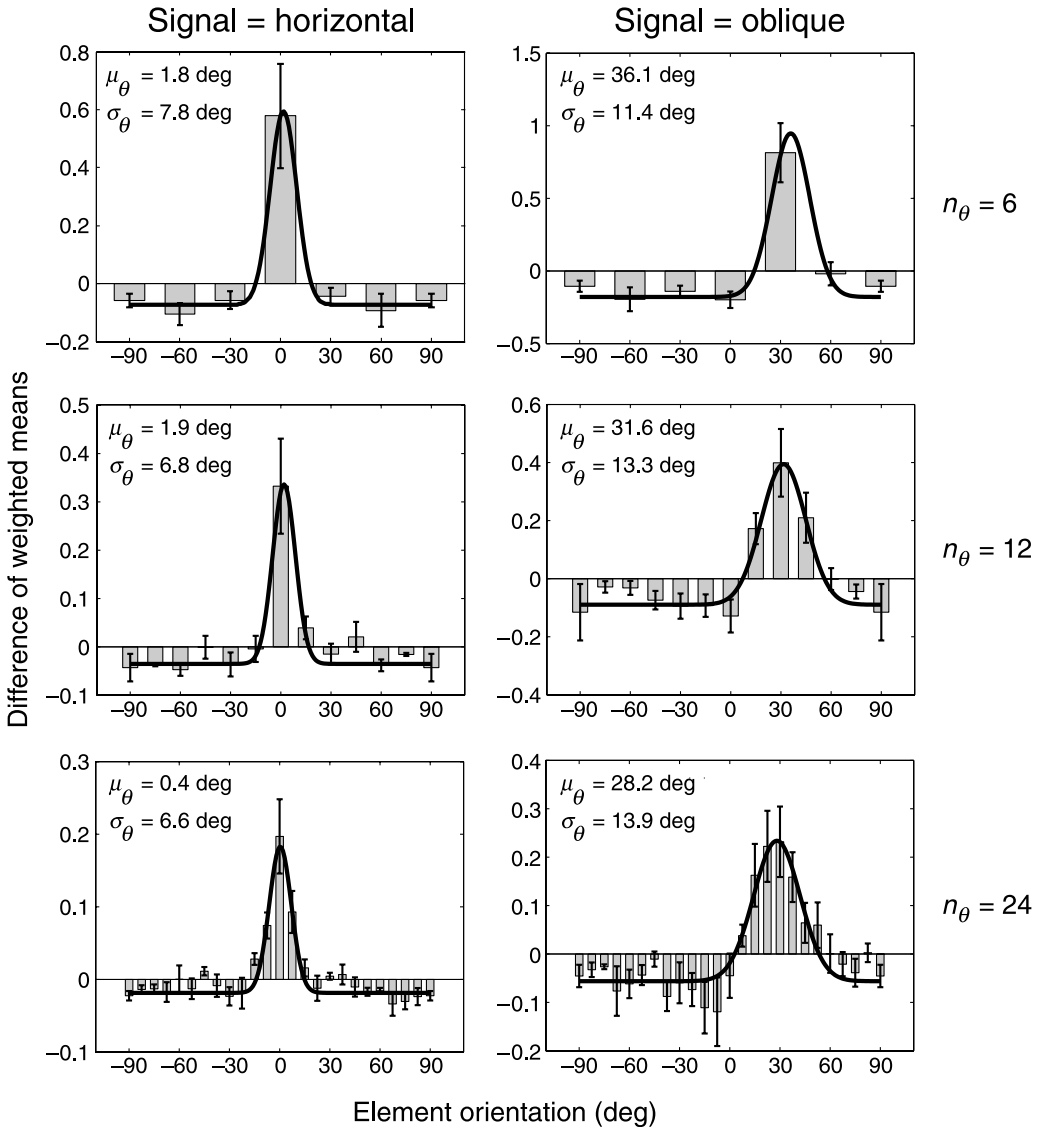

Figure 6. Empirical sensitivity function in the orientation domain. The curve in each plot shows the least-squares fit of the lowered Gaussian function (Equation 15), with parameters μ_θ and σ_θ. n_θ denotes the number of orientations in the stimulus. Error bars represent ±1 *SEM*. The mean and *SEM* for each orientation bin are derived from 6 estimates: 3 observers × 2 stimulus types.

for the two types of oriented elements, consistent with Dakin's (1997) psychophysical findings. Indeed, orientation-selective neurons in V1 and V2 have been shown to be sensitive to both Glass-pattern dipoles (Smith et al., 2002, 2007) and line textures (Kastner, De Weerd, & Ungerleider, 2000; Knierim & van Essen, 1992).

Orientation bandwidth was significantly greater for oblique stimuli than for horizontal stimuli, $F(1,7) = 10.4$, $p < 0.02$ (Figures 6 and 7). Superficially at least, this may seem like a surprising result, given that larger orientation bandwidth should lead to reduced detection performance, yet we generally find that observers are better at detecting oblique patterns (Figure 4). Combined with our analysis of eccentricity loss (Figure 5b), our results suggest that the inverse oblique effect is due to broader spatial pooling for oblique patterns and not to superior orientation tuning. Our results thus explain how the classical oblique effect (Jastrow, 1892) and the inverse oblique effect for Glass patterns are not inconsistent. Whereas the first effect is due to weaker orientation tuning for oblique signals, the latter is due to broader spatial pooling for oblique signals.

There were also differences among observers, $F(2,7) = 9.54$, $p < 0.02$ (Figure 7). A Tukey's post hoc pairwise comparison test revealed that only YM differed in his orientation bandwidth from the other two observers (YM vs. CFO: $p < 0.01$, YM vs. DN: $p < 0.05$, CFO vs. DN: $p = 0.48$). It is worth noting that YM also had a larger eccentricity loss (Figure 5b).

Downloaded from jov.arvojournals.org on 06/30/2019

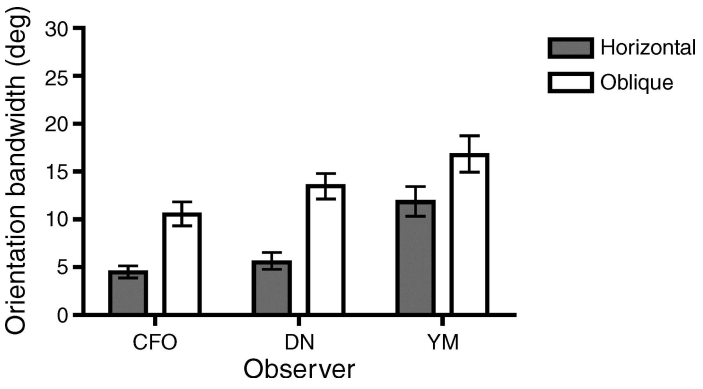

Figure 7. Orientation bandwidths σ_θ estimated from the 24-orientation conditions. Data were first pooled over stimulus types. Error bars represent 68% confidence intervals, estimated by bootstrapping from the original noise elements.

The average bandwidth over all conditions was σ_θ = 11.1 deg, consistent with Maloney et al.'s (1987) estimate of 11 deg for Glass patterns. Our estimate is equivalent to 13.1 deg, half-width at half-height, within the range of orientation bandwidths (7–15 deg) estimated from grating stimuli (Blakemore & Nachmias, 1971; Campbell & Kulikowski, 1966; Phillips & Wilson, 1984; Snowden, 1992).

Quantifying information loss

The observed decay in sensitivity with eccentricity and the apparent loss in orientation information must contribute to the elevation of human thresholds relative to the ideal. Here, we set out to quantify just how much of this performance gap can be explained in this way.

Eccentricity loss

To quantify the effects of eccentricity loss, we modified the ideal observer model (Ideal observer modelling section) to base its decision on a weighted sum of elements at the signal orientation, where weights w_j^e were given by the exponential model estimated in the Classification image analysis section. Specifically, given a stimulus with n_0 elements at the signal orientation, the modified ideal observer uses the decision variable:

$$\tilde{n}_0 = \sum_{j=1}^{n_0} w_j^e, \tag{16}$$

where $w_j^e = \exp(-r_j/r_0)$, and r_j is the eccentricity of the jth element at the signal orientation.

To determine the optimal criterion $\tilde{n}_0'$ of the modified ideal observer, we simulated 5000 signal-present trials for each possible value of the signal level $n_s \in [0, \ldots, N]$ and 5000 signal-absent trials, sampling the associated binomial distributions in each case (Equations 2 and 3) to determine values for n_0. Eccentricity values r_j for each of the n_0 elements at the signal orientation in a given trial were then simulated by sampling r_j^2 from a uniform distribution $[0, R^2]$, where R = 7 deg is the radius of the stimulus. The weights w_j^e and decision variable $\tilde{n}_0$ were then computed based on Equation 16.

The optimal criterion for each signal level $\tilde{n}_0'(n_s)$ was determined by maximizing the proportion of correct responses for this signal level. The model threshold for 75% correct performance was then estimated by linear interpolation.

Orientation loss

Modifications to the ideal observer to incorporate orientation loss were similar in spirit to the eccentricity modifications. We again simulated 5000 trials for every possible signal level and for both signal-absent and signal-present conditions. The orientations of each of the N = 200 elements in each stimulus were determined by setting n_s to the signal orientation and distributing the remaining $N - n_s$ according to a uniform distribution over all orientations to mimic the oriented textures generated for human observers (Stimuli section; Figure 3). The decision variable $\tilde{n}_0$ was then determined as

$$\tilde{n}_0 = \sum_{j=1}^{N} w_j^\theta, \tag{17}$$

where the weights w_j^θ were determined from the estimated Gaussian tuning function (Equation 15):

$$w_j^\theta = \exp\left(\frac{-(\theta_j - \mu_\theta)^2}{2\sigma_\theta^2}\right). \tag{18}$$

(We omit the normalizing term used in Equation 15, since it serves to subtract the same constant from the decision variable on each trial, thus having no effect on discrimination.) The optimal criterion for each signal level $\tilde{n}_0'(n_s)$ and threshold at 75% correct performance was then determined as in the Eccentricity loss section.

Downloaded from jov.arvojournals.org on 06/30/2019

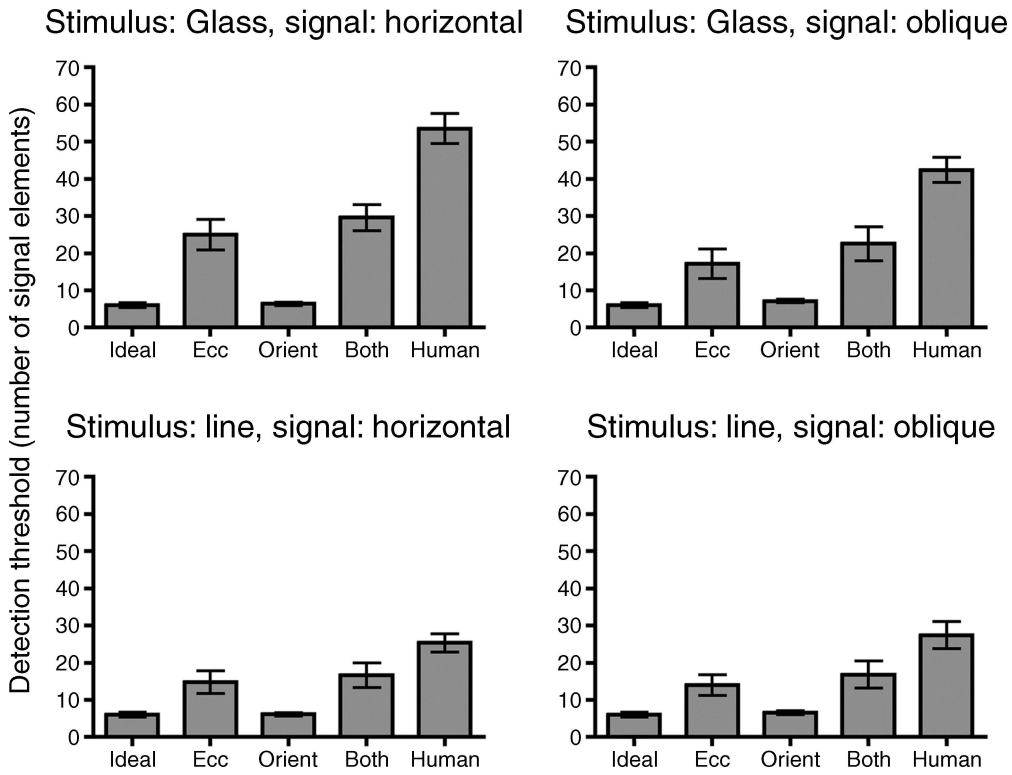

Figure 8. Detection thresholds for human and ideal observers, as well as modified versions of the ideal observer incorporating eccentricity losses (Ecc), orientation losses (Orient), or both losses together (Both). Error bars denote ±1 *SEM*. The mean and *SEM* for the ideal observer model are derived from 3 estimates, corresponding to the 3 values of the number of orientations factor. The mean and *SEM* for each of the other models and the human data are derived from 9 estimates: 3 observers × 3 number of orientations values.

Eccentricity loss and orientation loss

The effects of both eccentricity loss and orientation loss together were determined in a similar fashion, with decision variable $\tilde{n}_0$ given by

$$\tilde{n}_0 = \sum_{j=1}^{N} w_j^e w_j^\theta. \quad (19)$$

Results

Figure 8 shows detection thresholds for these modified ideal observer models, averaged over observers and numbers of orientations. Human thresholds for Glass patterns are, on average, 8.0 times greater than the ideal thresholds. While orientation losses alone increase thresholds by only 8% from the ideal, eccentricity losses increase ideal thresholds by a factor of 2.9. Interestingly, when orientation losses are combined with eccentricity losses, they seem to have a greater effect: Together they raise ideal thresholds by a factor of 3.5. By comparing human thresholds for Glass patterns and line patterns (Results section), we estimate that losses due to correspondence errors increase human thresholds by a factor of 1.8. The combined effect of these three sources of error (correspondence errors, eccentricity losses, orientation losses) can be taken into account by comparing the ideal observer model with both eccentricity and orientation losses to human thresholds for the line stimulus conditions (i.e., by comparing "Both" and "Human" thresholds for the two lower plots in Figure 8). We find that human thresholds are only 58% higher than model thresholds. This puts a useful upper bound on the effects of other potential sources of error (see below).

Discussion

Major factors limiting oriented texture detection

A number of factors appear to limit human oriented texture detection. Comparisons of human thresholds for Glass patterns and line patterns for the three observers confirm that correspondence errors are a major source of information loss, raising human thresholds by a factor of 1.8. Our ideal observer and classification image analysis reveals that, while eccentricity loss is also a major factor, the effect of orientation loss is negligible.

Downloaded from jov.arvojournals.org on 06/30/2019

Inverse oblique effect

Our findings of generally lower thresholds and larger space constants for oblique textures are consistent with the inverse oblique effect, as suggested by Wilson et al. (2001). Sensitivity to oblique textures is higher as the visual system appears to broaden the extent of spatial summation to extract the oblique textures, resulting in a larger space constant. The larger spatial summation apparently more than compensates for the weaker orientation tuning at oblique angles that underlies the well-known oblique effect. This explanation is supported by our finding that orientation loss has a relatively minor effect on performance compared to the loss associated with spatial pooling.

Deviations from assumptions underlying classification image analysis

The total number of signal and noise elements in each stimulus was fixed at 200 elements. Consequently, observations in each of the discrete orientations are not independent. For example, observing a large number of elements at a particular orientation lowers the numbers expected at other orientations. In other words, the noise in our experiment was not white, as is required in standard classification image analysis. In order to assess the impact of non-white noise, we conducted a control experiment on both Glass patterns and line patterns (horizontal signal, 24 orientations only) in which the number of noise elements at each orientation was drawn from an independent normal distribution with standard deviation $\sigma = 2.5$ elements and mean $\mu = (N - n_s) / n_\theta$ for signal-present trials and $\mu = N/n_\theta$ for signal-absent trials, where $N = 200$ is the *expected* total number of elements in the stimulus, n_s is the number of signal elements, and n_θ is the number of orientations ($n_\theta = 24$ in this case). The same three observers performed this experiment, and the other experimental setup was the same as previously described (Stimuli and Procedure sections). Note that the total number of elements in the stimulus now varies from trial to trial but is not predictive of the signal.

Figure 9 shows estimates of orientation tuning based on this experiment. A two-way repeated-measures ANOVA is performed to compare the estimates from using white noise and non-white noise based on the observer and the stimulus type factors. The result shows that neither main effects are significant (observer: $F(1,1) = 5.47$, $p = 0.26$; stimulus type: $F(1,1) = 0.027$, $p = 0.90$), and the interaction effect is also not significant ($F(1,1) = 2.20$, $p = 0.38$). Thus, orientation bandwidths estimated using white noise do not differ significantly from the original results based on fixing the total number of elements in the stimulus (Figure 10).

Prior knowledge of signal level

In constructing the ideal observer, we assumed knowledge of the signal level. Since we use an adaptive psychometric procedure (QUEST; Watson & Pelli, 1983), the signal level changes from trial to trial, and so it is highly unlikely that our human observers know the correct signal level on each trial. Thus, the assumption of perfect knowledge of signal level yields an upper bound on the performance (or lower bound on the threshold) of an observer that perceives the stimulus perfectly.

A possible alternative assumption is that the human observer has absolutely no knowledge of signal level, i.e., assumes a uniform prior over the possible values $n_s \in [1, \ldots,$

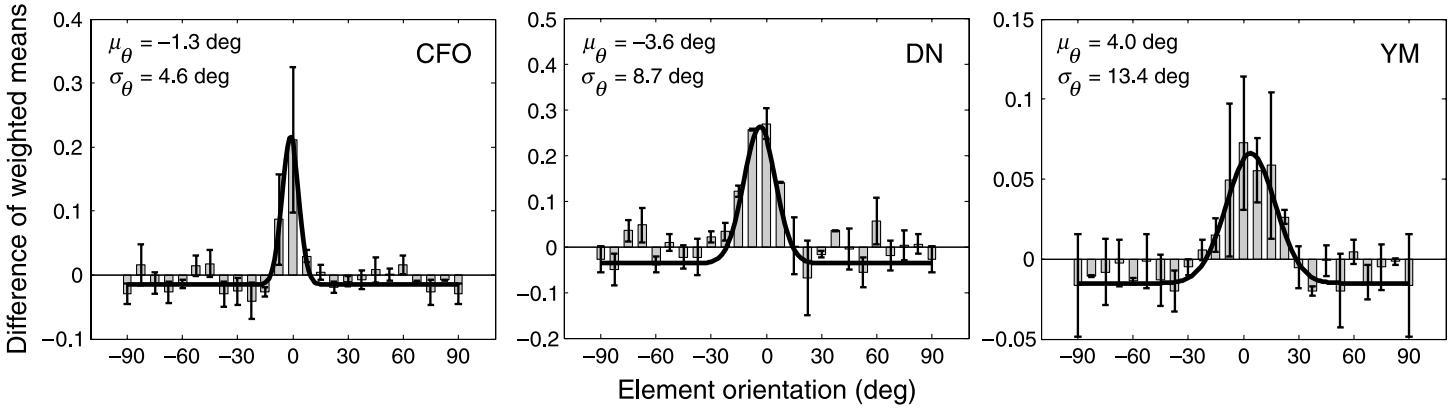

Figure 9. Empirical sensitivity functions over orientation from a control experiment (Deviations from assumptions underlying classification image analysis section) using white orientation noise, with maximum likelihood lowered Gaussian fits. The experiment used only stimuli with horizontal signal and 24 orientations. Error bars represent ±1 *SEM*. The mean and *SEM* for each orientation bin are derived from 2 estimates from 2 stimulus types.

Downloaded from jov.arvojournals.org on 06/30/2019

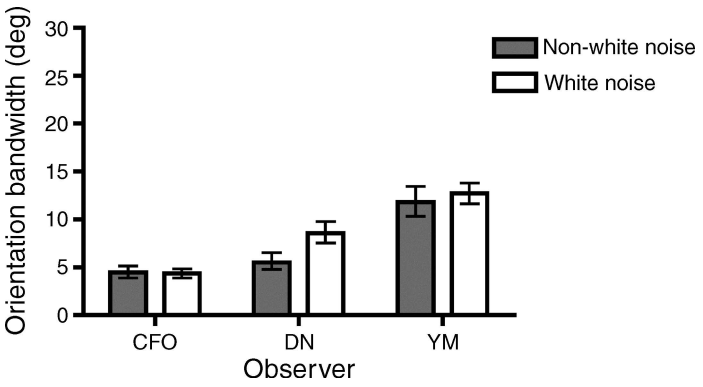

Figure 10. Orientation bandwidths σ_θ estimated from the original method (non-white orientation noise, Figure 7) and the control experiment (white orientation noise; see Deviations from assumptions underlying classification image analysis section) for stimuli with horizontal signal and 24 orientations. Data were first pooled over stimulus types. Error bars represent 68% confidence intervals, estimated by bootstrapping from the original noise elements.

N]. The expected signal level is then $(N + 1) / 2$ and the variance is

$$E\left[\left(n_s - \frac{N+1}{2}\right)^2\right] = \frac{1}{N}\sum_{n_s=1}^{N}\left(n_s - \frac{N+1}{2}\right)^2 = \frac{1}{12}(N^2 - 1). \quad (20)$$

For $N = 200$, the variance corresponds to a standard deviation of 57.7 elements. The resulting ideal observer model can be taken as a lower bound on the performance (or upper bound on the threshold) of an observer that perceives the stimulus perfectly.

The truth no doubt lies somewhere in the middle. In our experiments, we found that the QUEST procedure converged rapidly, so that the standard deviation of the signal level over each 200-trial block was in fact quite small, averaging only to 7.8 elements (Figure 11). Thus, a more reasonable assumption may be that the human observer applies a prior on the signal level with roughly

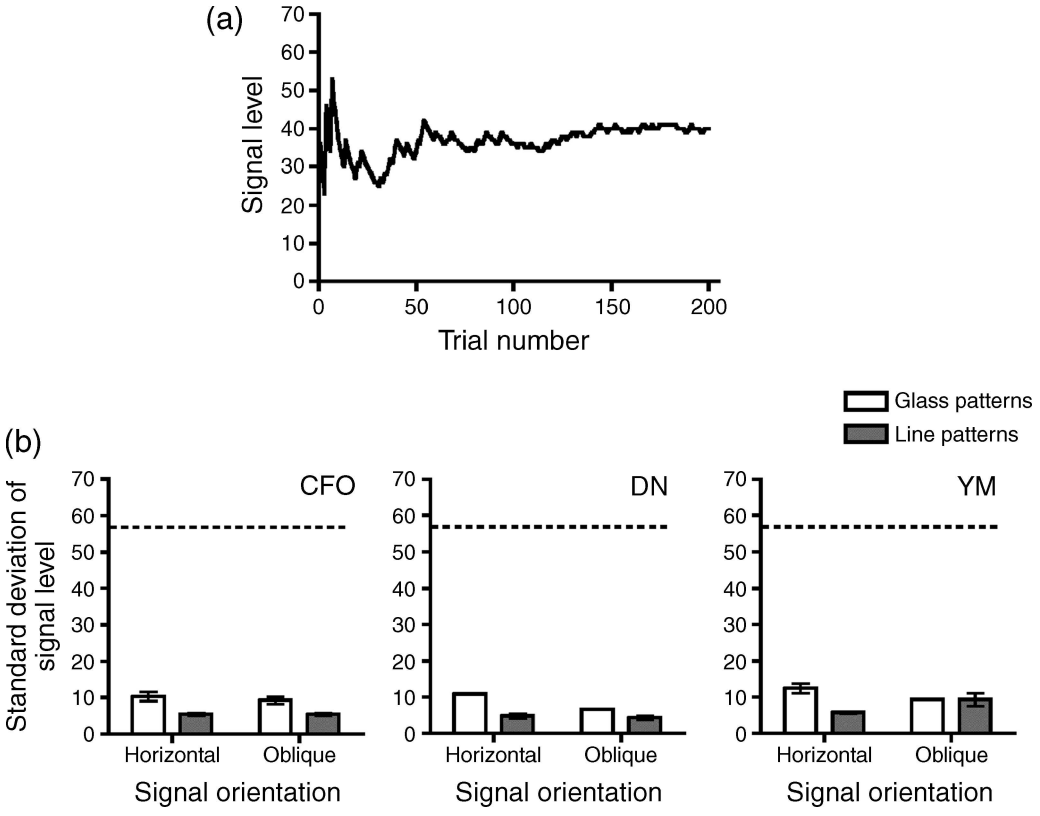

Figure 11. (a) A typical block of trials (observer DN, horizontal Glass patterns, 24 orientations) showing the convergence of the signal level over time. (b) The mean and *SEM* of the standard deviation of the signal level over a block, averaged over all values of the number of orientations factor. Error bars represent ±1 *SEM*. The dotted line in each plot shows the standard deviation for a uniform prior over signal level (Equation 20).

Downloaded from jov.arvojournals.org on 06/30/2019

the correct mean and the variance matching the empirical variance over a block of trials.

We can use the methods of the Ideal observer modelling section to compute the ideal observer performance under these different assumptions. This requires only a modification to the signal-present distribution over n_0 (Equation 2) to marginalize over the unknown signal level n'_s:

$$p(n_0|H_1) = \sum_{n'_s=1}^{n_0} p(n'_s) \binom{N - n'_s}{n_0 - n'_s} p_\theta^{n_0 - n'_s} (1 - p_\theta)^{N - n_0}, \quad (21)$$

where $p(n'_s)$ is the prior over n'_s. For the uniform prior (lower bound), this becomes

$$p(n_0|H_1) = \frac{1}{N} \sum_{n'_s=1}^{n_0} \binom{N - n'_s}{n_0 - n'_s} p_\theta^{n_0 - n'_s} (1 - p_\theta)^{N - n_0}. \quad (22)$$

For the matched-variance prior, we assume a normal distribution:

$$p(n_0|H_1) = \sum_{n'_s=1}^{n_0} \mathcal{N}(n'_s; n_s, \sigma^2_{n_s}) \binom{N - n'_s}{n_0 - n'_s} p_\theta^{n_0 - n'_s} (1 - p_\theta)^{N - n_0}. \quad (23)$$

where n_s is the true signal level and $\sigma^2_{n_s}$ is the empirical variance in the signal level over a block.

Figure 12 shows how the three variations on the ideal observer perform. We find that assuming a flat prior raises the ideal threshold by 97% on average. Recall that human thresholds are only 58% higher than the ideal once correspondence errors, eccentricity, and orientation losses are factored in. This provides strong evidence that human observers have some prior knowledge of the signal level. In contrast, a more reasonable matched-variance prior raises the ideal threshold by only 16% on average. We thus estimate that imperfect knowledge of the signal may account for approximately 27% of the remaining information loss.

Other factors

Our results suggest that beyond correspondence errors, eccentricity loss, and orientation loss, there are other errors underlying oriented texture detection yet to be understood. One possibility is response bias. However, log-likelihood response biases averaged only 0.08, and taking the biases into account raised ideal observer thresholds by only 1% on average.

Another potential error is mutual modulations of orientation signals arising from neighbouring elements in an oriented texture (Verghese, 2001), during the process of integrating local orientation signals into a global percept. When an element is surrounded by many other elements, orientation detection of that element may be modulated by orientation signals from nearby elements. If these modulations are not orientation-specific, they will lower performance on the task but will not broaden the approximately Gaussian tuning to the signal orientation apparent in the classification image and, thus, will not be taken into account by our model.

The sources of error we have modelled are deterministic, given the stimuli, but there are no doubt also random sources of error caused by various kinds of internal noise.

Relation to prior work

Prior work on the detection and discrimination of oriented texture patterns is generally based on the measurement of psychophysical thresholds as a function of stimulus parameters such as the spatial extent of the

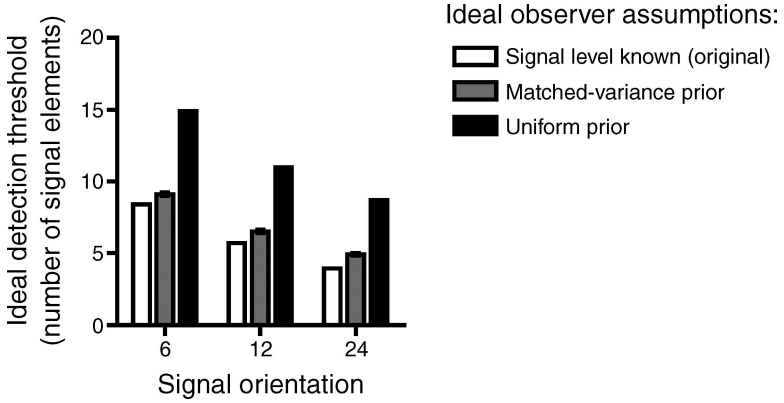

Figure 12. Detection thresholds for three versions of the ideal observer with different levels of knowledge about the signal level (Prior knowledge of signal level section). Thresholds for the matched-variance prior are averaged over 12 conditions (3 observers × 2 stimulus types × 2 signal orientations). Error bars denote ±1 *SEM* derived from these averages.

Downloaded from jov.arvojournals.org on 06/30/2019

texture and the variance of orientation noise added to the elements (e.g., Beaudot & Mullen, 2006; Dakin, 1997, 2001; Wilson & Wilkinson, 1998). While we also measure detection thresholds as a function of certain parameters (stimulus type, signal orientation, number of orientations), we use classification image analysis to identify parameters for spatial integration and orientation tuning. This technique has certain advantages. Fewer conditions are needed for our method, since neither the spatial extent nor the distribution of noise elements is varied. In addition, in the standard psychophysical method, an implicit assumption must be made that the spatial and orientation bandwidth parameters of detection/discrimination mechanisms remain invariant as the stimulus parameters change. This assumption need not be made in our method, since the spatial extent and orientation distributions remain the same.

Given the differences between the methods, it is reassuring that prior studies yield similar estimates for the falloff in sensitivity with eccentricity (Wilson & Wilkinson, 1998) and orientation bandwidth (Blakemore & Nachmias, 1971; Campbell & Kulikowski, 1966; Dakin, 1997, 2001; Maloney et al., 1987; Phillips & Wilson, 1984; Snowden, 1992) and that we see evidence for the inverse oblique effect (Wilson et al., 2001).

One novel result is that, while we see broader spatial integration for oblique patterns, as previously reported (Wilson et al., 2001), we also see broader orientation tuning for these patterns, as predicted by the classical oblique effect. While the latter effect would predict lower performance for oblique patterns, our analysis of the information losses entailed by subideal spatial and orientation tuning reveals that these losses put overwhelming constraints on spatial integration that limit processing of oriented textures. Thus, the inverse oblique effect dominates the classical oblique effect in the global processing of oriented textures.

Prior modelling work on the discrimination of oriented texture patterns has yielded estimates of (late) internal orientation noise and the effective number of independent orientation samples on which discrimination is based

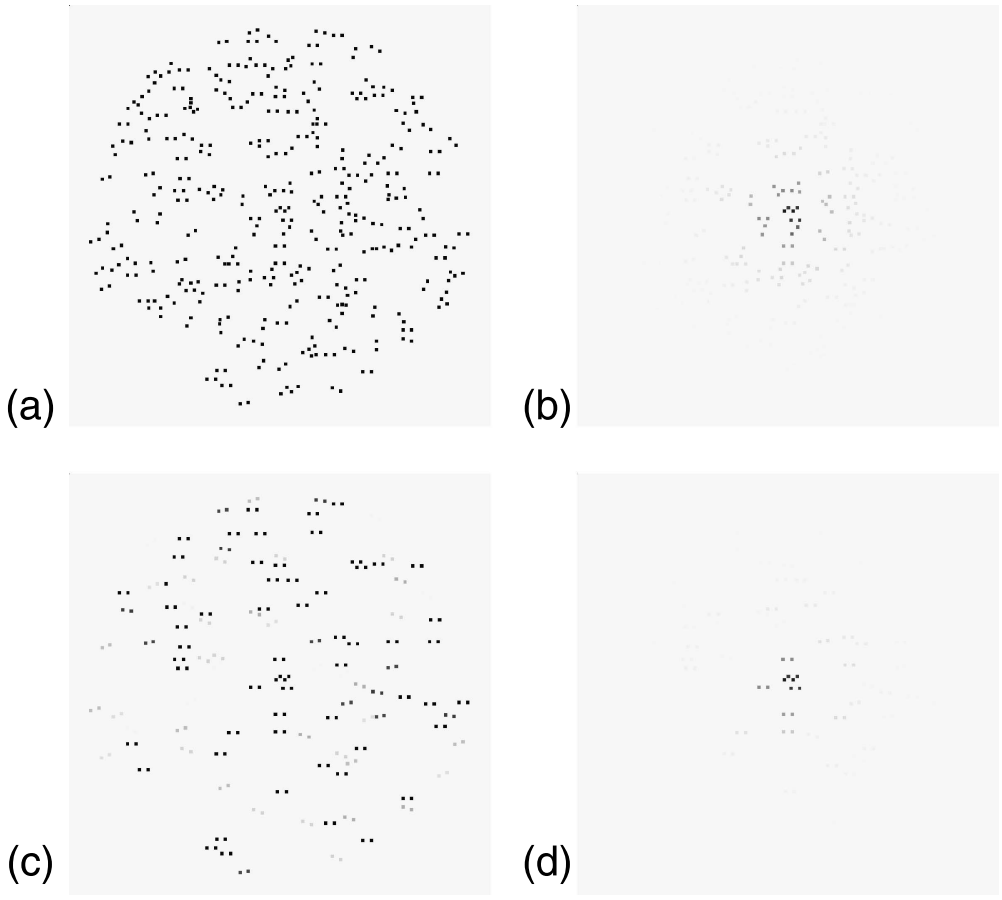

Figure 13. The role of eccentricity and orientation filtering in Glass pattern detection. For illustration purposes only, we set the contrast of each dipole to match its estimated perceptual weight in determining the detection response. (a) Horizontal Glass pattern with 27% signal level, the average detection threshold over observers for this condition. The same Glass patterns attenuated in contrast for (b) eccentricity filtering only, (c) orientation filtering only, and (d) both eccentricity and orientation filtering. The eccentricity space constant of 0.81 deg and orientation bandwidth of 10.2 deg represent the means of estimates over observers, derived from our classification image analysis (Classification image analysis section) for horizontal Glass patterns.

Downloaded from jov.arvojournals.org on 06/30/2019

(Dakin, 2001). While we model orientation selectivity as deterministic, our data do not, in fact, distinguish between this form of sampling inefficiency and internal orientation noise, although an additional double-pass experiment (Burgess & Colborne, 1988) could, in principle, distinguish the two.

More recent work has focused on possibly non-linear centre–surround normalization mechanisms that may play a role (Beaudot & Mullen, 2006). Our results do not speak directly to this. Instead, we have tried to construct models derived from the ideal that make as few assumptions as possible, in order to establish a firmer bound on the efficiency of oriented texture detection, taking into account measured losses due to correspondence error and limits on spatial integration and orientation acuity. We arrive at the result that, when taking these known losses into account, human thresholds are only 58% higher than the ideal. Any additional losses, for example, due to local normalization mechanisms, should respect this bound.

Visualizing information loss

Figure 13 provides a visualization of the effects of eccentricity and orientation losses. A sample signal-present stimulus near human threshold is shown. For illustration purposes only, we selectively attenuated the contrast of each dipole to match its estimated perceptual weight in determining the detection response, reflecting eccentricity and orientation losses. It is striking how little of the stimulus determines human judgments when both sources of information loss are taken into account.

Acknowledgments

We thank Richard Murray for his helpful comments. This work was supported by CIHR, GEOIDE, NSERC, OCE, and PREA. The image of the squirrel was granted for use by English Country Garden (http://www.english-country-garden.com).

Commercial relationships: none.
Corresponding author: Charles C.-F. Or.
Email address: cfor@yorku.ca.
Address: Centre for Vision Research, York University, 4700 Keele Street, Toronto, ON, Canada.

References

Abbey, C. K., & Eckstein, M. P. (2002). Classification image analysis: Estimation and statistical inference for two-alternative forced-choice experiments. *Journal of Vision, 2*(1):5, 66–78, http://www.journalofvision.org/content/2/1/5, doi:10.1167/2.1.5. [PubMed] [Article]

Ahumada, A. J., Jr. (2002). Classification image weights and internal noise level estimation. *Journal of Vision, 2*(1):8, 121–131, http://www.journalofvision.org/content/2/1/8, doi:10.1167/2.1.8. [PubMed] [Article]

Ahumada, A. J., Jr., & Beard, B. L. (1999). Classification images for detection [ARVO Abstract]. *Investigative Ophthalmology and Visual Science, 40,* S572.

Ahumada, A. J., Jr., & Lovell, J. (1971). Stimulus features in signal detection. *Journal of the Acoustical Society of America, 49,* 1751–1756.

Beaudot, W. H. A., & Mullen, K. T. (2006). Orientation discrimination in human vision: Psychophysics and modeling. *Vision Research, 46,* 26–46.

Blakemore, C., & Nachmias, J. (1971). The orientation specificity of two visual after-effects. *The Journal of Physiology, 213,* 157–174.

Burgess, A. E., & Colborne, B. (1988). Visual signal detection. IV. Observer inconsistency. *Journal of the Optical Society of America A, 5,* 617–627.

Burr, D., & Ross, J. (2006). The effects of opposite-polarity dipoles on the detection of Glass patterns. *Vision Research, 46,* 1139–1144.

Caelli, T. M. (1981). Some psychophysical determinants of discrete Moiré patterns. *Biological Cybernetics, 39,* 97–103.

Campbell, F. W., & Green, D. G. (1965). Optical and retinal factors affecting visual resolution. *The Journal of Physiology, 181,* 576–593.

Campbell, F. W., & Kulikowski, J. J. (1966). Orientational selectivity of the human visual system. *The Journal of Physiology, 187,* 437–445.

Cowey, A., & Rolls, E. T. (1974). Human cortical magnification factor and its relation to visual acuity. *Experimental Brain Research, 21,* 447–454.

Dakin, S. C. (1997). The detection of structure in Glass patterns: Psychophysics and computational models. *Vision Research, 37,* 2227–2246.

Dakin, S. C. (2001). Information limit on the spatial integration of local orientation signals. *Journal of the Optical Society of America A, Optics, Image Science, and Vision, 18,* 1016–1026.

Dakin, S. C., & Bex, P. J. (2001). Local and global visual grouping: Tuning for spatial frequency and contrast. *Journal of Vision, 1*(2):4, 99–111, http://www.journalofvision.org/content/1/2/4, doi:10.1167/1.2.4. [PubMed] [Article]

Daniel, P. M., & Whitteridge, D. (1961). The representation of the visual field on the cerebral cortex in monkeys. *The Journal of Physiology, 159,* 203–221.

Downloaded from jov.arvojournals.org on 06/30/2019

De Monasterio, F. M., & Gouras, P. (1975). Functional properties of ganglion cells of the rhesus monkey retina. *The Journal of Physiology, 251,* 167–195.

Fincham, E. F. (1951). The accommodation reflex and its stimulus. *British Journal of Ophthalmology, 35,* 381–393.

Glass, L. (1969). Moiré effects from random dots. *Nature, 223,* 578–580.

Glass, L., & Pérez, R. (1973). Perception of random dot interference patterns. *Nature, 246,* 360–362.

Glass, L., & Switkes, E. (1976). Pattern recognition in humans: Correlations which cannot be perceived. *Perception, 5,* 67–72.

Hubel, D. H., & Wiesel, T. N. (1962). Receptive fields, binocular interaction and functional architecture in the cat's visual cortex. *The Journal of Physiology, 160,* 106–154.

Hubel, D. H., & Wiesel, T. N. (1968). Receptive fields and functional architecture of monkey striate cortex. *The Journal of Physiology, 195,* 215–243.

Jastrow, J. (1892). On the judgment of angles and positions of lines. *American Journal of Psychology, 5,* 214–248.

Kastner, S., De Weerd, P., & Ungerleider, L. G. (2000). Texture segregation in the human visual cortex: A functional MRI study. *Journal of Neurophysiology, 83,* 2453–2457.

Knierim, J. J., & van Essen, D. C. (1992). Neuronal responses to static texture patterns in area V1 of the alert macaque monkey. *Journal of Neurophysiology, 67,* 961–980.

Kurki, I., Laurinen, P., Peromaa, T., & Saarinen, J. (2003). Spatial integration in Glass patterns. *Perception, 32,* 1211–1220.

Maloney, R. K., Mitchison, G. J., & Barlow, H. B. (1987). Limit to the detection of Glass patterns in the presence of noise. *Journal of the Optical Society of America A, Optics, Image Science, and Vision, 4,* 2336–2341.

Phillips, G. C., & Wilson, H. R. (1984). Orientation bandwidths of spatial mechanisms measured by masking. *Journal of the Optical Society of America A, Optics and Image Science, 1,* 226–232.

Robson, J. G., & Graham, N. (1981). Probability summation and regional variation in contrast sensitivity across the visual field. *Vision Research, 21,* 409–418.

Smith, M. A., Bair, W., & Movshon, J. A. (2002). Signals in macaque striate cortical neurons that support the perception of Glass patterns. *Journal of Neuroscience, 22,* 8334–8345.

Smith, M. A., Kohn, A., & Movshon, J. A. (2007). Glass pattern responses in macaque V2 neurons. *Journal of Vision, 7*(3):5, 1–15, http://www.journalofvision.org/content/7/3/5, doi:10.1167/7.3.5. [PubMed] [Article]

Snowden, R. J. (1992). Orientation bandwidth: The effect of spatial and temporal frequency. *Vision Research, 32,* 1965–1974.

Spinelli, D., Bazzeo, A., & Vicario, G. B. (1984). Orientation sensitivity in the peripheral visual field. *Perception, 13,* 41–47.

Stevens, K. (1978). Computation of locally parallel structure. *Biological Cybernetics, 6,* 19–28.

Verghese, P. (2001). Visual search and attention: A signal detection theory approach. *Neuron, 31,* 523–535.

Watson, A. B., & Pelli, D. G. (1983). QUEST: A Bayesian adaptive psychometric method. *Perception & Psychophysics, 33,* 113–120.

Wiesel, T. N. (1960). Receptive fields of ganglion cells in the cat's retina. *The Journal of Physiology, 153,* 583–594.

Wilson, H. R., Loffler, G., Wilkinson, F., & Thistlethwaite, W. A. (2001). An inverse oblique effect in human vision. *Vision Research, 41,* 1749–1753.

Wilson, H. R., & Wilkinson, F. (1998). Detection of global structure in Glass patterns: Implications for form vision. *Vision Research, 38,* 2933–2947.

Wilson, H. R., Wilkinson, F., & Asaad, W. (1997). Concentric orientation summation in human form vision. *Vision Research, 37,* 2325–2330.

Downloaded from jov.arvojournals.org on 06/30/2019